UV, visible and near-infrared lights induced NO$_x$ destruction activity of (Yb,Er)-NaYF$_4$/C-TiO$_2$ composite

Xiaoyong Wu[1], Shu Yin[1], Qiang Dong[1], Bin Liu[2], Yuhua Wang[2], Tohru Sekino[1], Soo Wohn Lee[3] & Tsugio Sato[1]

[1]Institute of Multidisciplinary Research for Advanced Materials, Tohoku University, 2-1-1, Katahira, Aoba-ku, Sendai 980-8577, Japan, [2]Lanzhou University, 222, Tianshuinan Road, Lanzhou 730000, People's Republic of China, [3]Sunmoon University, 100, GalSan-Ri, TangJung-Myon, Asan, ChungNam, 336-708, Republic of Korea.

Titanium dioxide (TiO$_2$) is a well-known photocatalyst for environmental cleaning and energy conversion. However, it can only be excited by ultraviolet light for photocatalysis due to its wide band gap (3.2 eV). In this paper, we present a novel (Yb,Er)-NaYF$_4$/C-TiO$_2$ composite which can be perfectly induced not only by ultraviolet light but also weak visible and near infrared lights, owing to the increased carbon doping contents and optimal energy transfer between up-conversion phosphor and C doped TiO$_2$ compared with that of solely C-TiO$_2$. Consequently, the (Yb,Er)-NaYF$_4$/C-TiO$_2$ composite can present the outstanding continuous NO$_x$ gas destruction ability under the irradiation of ultraviolet, weak visible and infrared lights much superior to pure C-TiO$_2$, P25 titania and even that of (Yb,Er)-NaYF$_4$/N-TiO$_2$ composite, due to the nice synergetic effect of (Yb,Er)-NaYF$_4$ and C-TiO$_2$, indicating a promising potential in the photocatalyst application with high efficiency of ultraviolet, visible and infrared lights induced photocatalysis simultaneously.

T iO$_2$, one of the most promising photocatalysts, has attracted considerable attention in recent years due to its high oxidative power, abundance, chemical stability, environmentally friendly and low cost[1–5]. Unfortunately, the wide band gap of TiO$_2$ ca. 3.2 eV has limited its widespread application in industry since it needs to be excited by ultraviolet (UV) light[6–8]. It is well known that the UV light only occupies 5% of solar light, whereas the residual 45% and 50% of solar light are comprised by visible light and near-infrared (NIR) light, respectively. Therefore, there is still a large space for TiO$_2$ to be improved for photocatalysis using solar light[9,10].

In order to overcome this issue, several strategies, such as dye sensitizing[11,12], heterostructure[13,14], ion doping[15–17], etc. have been developed. For example, Geneviève et al. reported that the visible solar light absorption of titanium dioxide could be significantly enhanced by combining titanium dioxide with Osmium and Ruthenium prolypyr-idyl complexes[18]. Zhou et al. presented that the visible light absorption of TiO$_2$ was able to be extended to 650 nm by forming a heterostructure with Ag$_2$O nanoparticles[19]. Yin et al. demonstrated that different phases of nitrogen doped titania nanocrystals were successfully prepared by a homogeneous precipitation-solvothermal process in TiCl$_3$-hexamethylenetetramine aqueous and alcohol solutions, and the as-prepared samples showed excellent visible light absorption due to the nitrogen doping in titania lattice[20]. However, most of them can only extend the solar light absorption of TiO$_2$ to the visible-light range. As for NIR light absorption, few papers reported about this. Qin group firstly demonstrated NIR-driven photocatalysis of TiO$_2$ by combining it with YF$_3$: Yb, Tm or NaYF$_4$: Yb,Tm[9,10]. The mechanism for this NIR-driven photocatalysis is as follows. The up-conversion phosphor absorbed the NIR light and then emitted UV light. Finally, this converted UV light would be reabsorbed by TiO$_2$ for photocatalysis. Nevertheless, in this case, only UV and NIR lights could be utilized by these two composites. Furthermore, the light conversion from NIR light to UV light is usually not efficient enough compared with the transformation from NIR light to visible light. Because the light energy conversion would be more efficient when the fewer anti-stokes shift was happened in this process[21–23]. Therefore, the combination of weak visible light induced TiO$_2$ based photocatalyst with NIR-Vis up-conversion phosphor obtaining the lower anti-stokes shift may be the more promising way to effectively use the whole solar light (UV, visible, NIR lights) for photocatalysis.

It is well known that NaYF$_4$ has been widely recognized as the most efficient host for up-conversion phosphor until now due to its low phonon energy and efficient multicolor emissions. Subsequently, the Yb and Er co-doped

$NaYF_4$ designated as (Yb,Er)-$NaYF_4$ has become the most promising visible light emitting up-conversion phosphor with two main emission peaks at about 545 and 655 nm under the irradiation of 980 nm[24–26]. In order to use (Yb,Er)-$NaYF_4$ as NIR-Vis conversion matrix achieving the optimal synergetic effect between up-conversion phosphor and photocatalyst, a suitable TiO_2 based photocatalyst, which has a good visible absorption covered the 545 and 655 nm range sufficiently, together with excellent photocatalytic activity under very weak light irradiation, is required.

Recently, C has become one of the most studied dopants in TiO_2[27,28] since Sakthivel et al. reported that carbon doped particles presented five times higher activity than nitrogen-doped TiO_2 in the degradation of 4-chlorophenol by visible light[29]. According to the density functional theory calculations within the generalized gradient approximation reported by Valentin et al[30]. C doped TiO_2 presented excellent visible light absorption and could cover the majority of visible solar lights by introducing series of localized occupied states above the valence band gap of TiO_2 semiconductor, and it has been experimentally confirmed by many researchers[27,31]. Our groups[32] also prepared the C doped TiO_2 by a facile solvothermal method, which exhibited fabulous visible light absorption in the range of 380–780 nm and corresponding nice visible light responsive NO_x destruction ability superior to that of N-TiO_2.

Therefore, in order to improve solar energy utilization by enabling the effective use of not only UV, visible lights but also NIR light for photocatalysis, a novel composite, which consisted of NIR light induced (Yb,Er)-$NaYF_4$ up-conversion phosphor and UV, visible lights driven C-TiO_2 photocatalyst, was synthesized by a facile calcination assisted solvothermal method without the addition of any other carbon precursors except for Ti source and ethanol solvent. In addition, the NO_x gas destruction activity was employed to test the photocatalytic ability of composite instead of dye solution degradation due to the influence of solution on the emission intensity of up-conversion phosphor, and also the week power of LEDs and infrared laser were used as irradiation sources to investigate the high efficiency of photocatalytic performance of the as-prepared samples more efficiently. More importantly, the photocatalytic stability and the effect of (Yb,Er)-$NaYF_4$ up-conversion phosphor on the total photocatalytic activity of (Yb,Er)-$NaYF_4$/C-TiO_2 composite under the irradiation of UV, visible, NIR lights, comparing with that of pure C-TiO_2 photocatalyst, should be the key points in the consideration of effective utilization of solar light for the enhanced photocatalysis.

Results

Characterization of samples. Figure 1 shows the XRD patterns of samples of C-TiO_2, (1:1)@(Yb,Er)-$NaYF_4$/C-TiO_2 and (Yb,Er)-$NaYF_4$. All the diffraction peaks of sample C-TiO_2 were well indexed to the anatase phase of TiO_2 (JCPDS file No. 21-1272) and no impurity peaks appeared. After combining with (Yb,Er)-$NaYF_4$ phosphor by a facile solvothermal method, no impurity peaks appeared in (1:1)@(Yb,Er)-$NaYF_4$/C-TiO_2 except for those of anatase TiO_2 and (Yb,Er)-$NaYF_4$, indicating that the introduction of (Yb,Er)-$NaYF_4$ in the solution made no visible change on the formation of anatase TiO_2 during the solvothermal process. The corresponding XRD patterns for other weight ratios of the composites are shown in supplementary Figure S1 and no difference was exhibited among them except for relative peak intensities.

Figure 2 shows the TEM image, HRTEM image, element mapping and EDX spectrum of (1:1)@(Yb,Er)-$NaYF_4$/C-TiO_2 composite. It could be clearly seen from element mapping that the element of Na, Y, F, Yb, Er, Ti and O truly existed in the sample. The element mapping of C is not shown because a large amount of C existed in the support film of the TEM grid. However, actually, the existence of C in the TiO_2 could be confirmed from the EDX spectrum and the following DRS and XPS analysis. In addition, it could also be found in Figure 2 that the large particle size of (Yb,Er)-$NaYF_4$ (200–400 nm) were successfully coated by small particles of C-TiO_2 (7–10 nm) to form core/shell structure. The d-spacing of covered small particle was about 0.351 nm, which agreed with the spacing of (101) of anatase TiO_2. The specific surface area of C-TiO_2 and (Yb,Er)-$NaYF_4$ were determined as 124.3 and 11.5 m^2g^{-1}, respectively. When the C-TiO_2 nanoparticles were combined with (Yb,Er)-$NaYF_4$ powders in core/shell structure, the specific surface was changed to 70.1 m^2g^{-1}. In addition, the SEM images of the samples C-TiO_2, (Yb,Er)-$NaYF_4$ and (1:1)@(Yb,Er)-$NaYF_4$/C-TiO_2 were also characterized (see supplementary Figure S2). After coupling small nanosize particle of C-TiO_2, the morphology and particle size of (1:1)@(Yb,Er)-$NaYF_4$/C-TiO_2 composite presented no big variation compared with those of solely (Yb,Er)-$NaYF_4$ except for a rough surface due to the covering of C-TiO_2 nanoparticles.

Figure 3 presents the DRS, PL spectra, visual emitting map of C-TiO_2, (1:1)@(Yb,Er)-$NaYF_4$/TiO_2, (1:1)@(Yb,Er)-$NaYF_4$/C-TiO_2 and (Yb,Er)-$NaYF_4$. It was apparent that C-TiO_2 exhibited a nice visible light absorption up to about 600 nm due to the C doping in TiO_2 by inducing some impurity energy levels of C above the valence band of TiO_2 (Figure 3 (a))[30,31]. (Yb,Er)-$NaYF_4$ displayed only the absorption band from 908 to 1028 nm, corresponding to the $^2F_{7/2} \rightarrow$ $^2F_{5/2}$ transition of Yb^{3+} in $NaYF_4$[33,34]. When TiO_2 was combined with (Yb,Er)-$NaYF_4$, (1:1)@(Yb,Er)-$NaYF_4$/TiO_2 represented a strong UV absorption of TiO_2 with the NIR light absorption band of (Yb,Er)-$NaYF_4$. Furthermore, (1:1)@(Yb,Er)-$NaYF_4$/C-TiO_2 showed the significantly enhanced visible light absorption up to 900 nm, owing to the introduction of C into TiO_2 lattice during calcination[35,36]. In addition, it is interesting that the visible light absorption of (1:1)@(Yb,Er)-$NaYF_4$/C-TiO_2 was much stronger than that of pure C-TiO_2, which is probably attributed to the increased C doping contents in TiO_2 in the presence of (Yb,Er)-$NaYF_4$ crystal. This phenomenon was also observed in our precious works[36]. The doped C contents in TiO_2 would be increased when other impurity ions (Nd^{3+}, etc.) or other phases were existed in the preparation of C-TiO_2 by solvothermal method. The advisable reason for this phenomenon is still unclear which will be our next work. The effects of (Yb,Er)-$NaYF_4$ contents on the DRS of (Yb,Er)-$NaYF_4$/C-TiO_2 composites are demonstrated in supplementary Figure S3. It was obvious that the
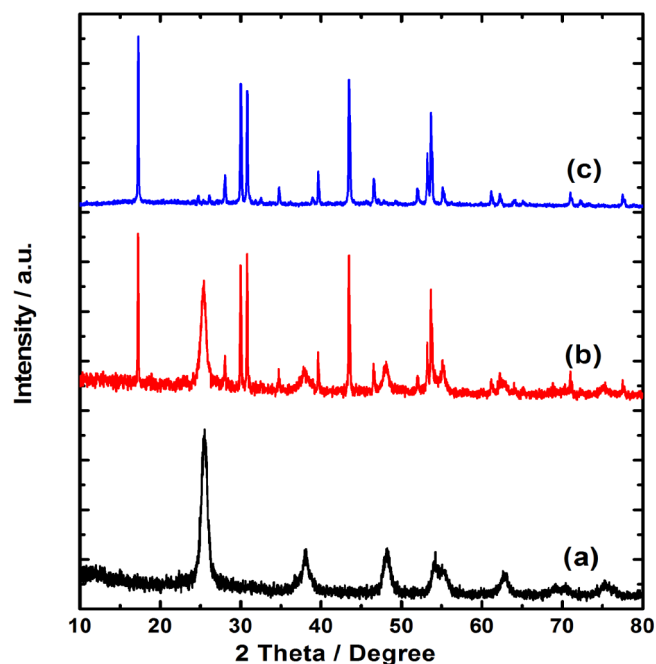

Figure 1 | XRD patterns of samples of (a) C-TiO_2, (b) (1:1)@(Yb,Er)-$NaYF_4$/C-TiO_2, (c) (Yb,Er)-$NaYF_4$.
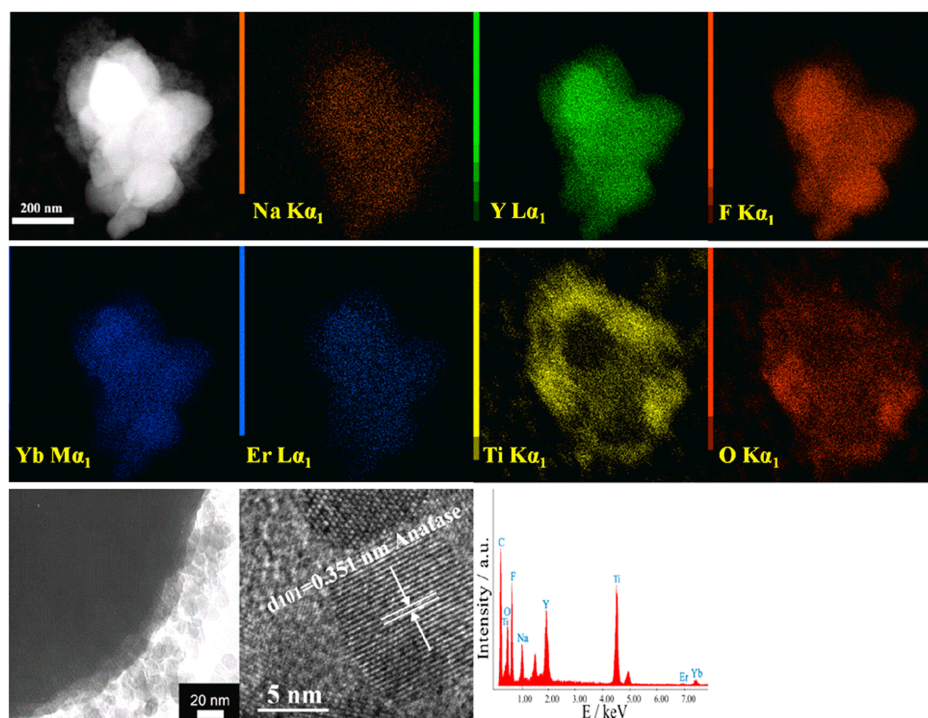
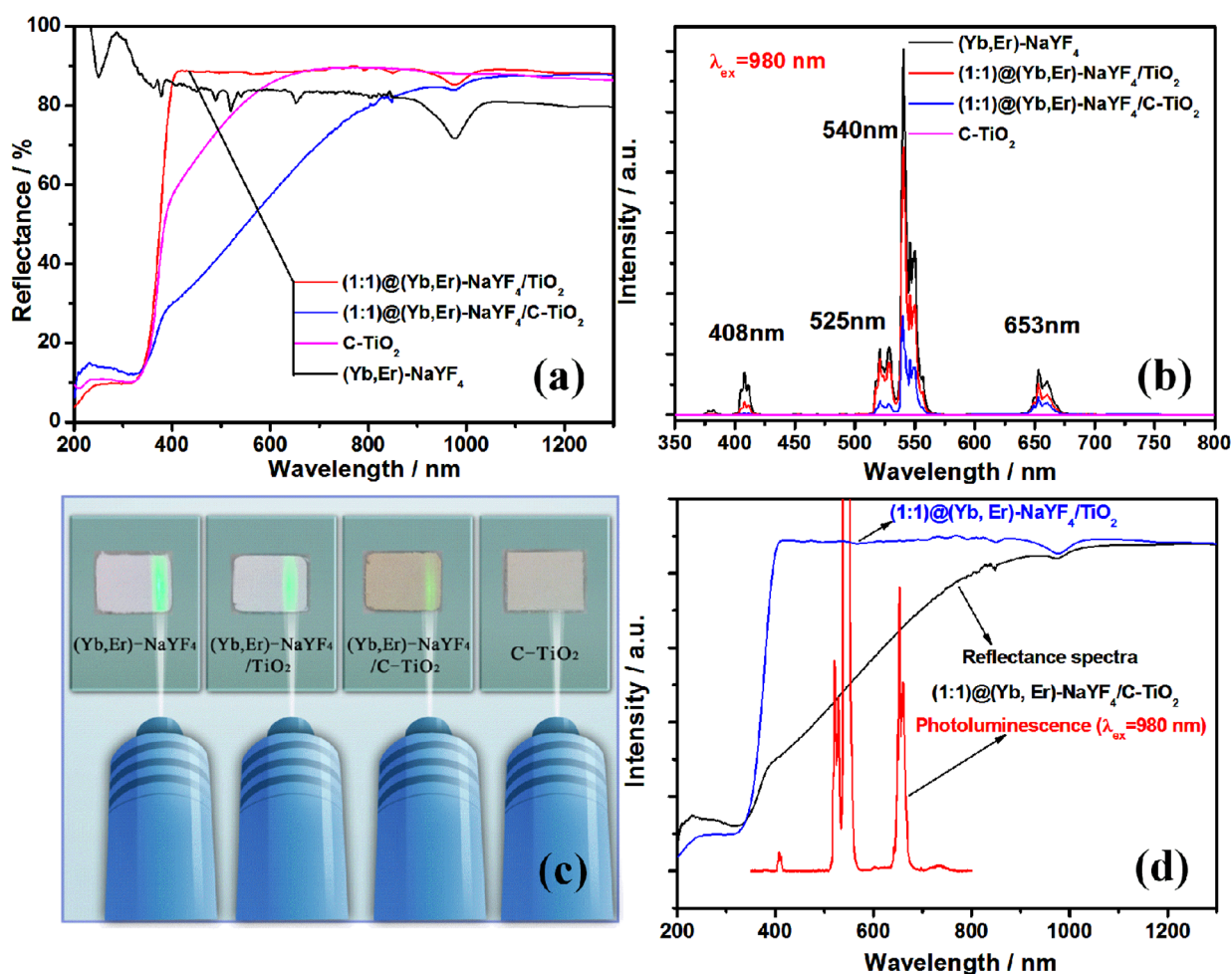**Figure 2 | Element mapping, TEM image, HRTEM image and EDX spectrum of the sample (1 : 1)@(Yb,Er)-NaYF$_4$/C-TiO$_2$.**

Figure 3 | DRS(a), PL spectra(b), visual emitting map(c) of C-TiO$_2$, (1 : 1)@(Yb,Er)-NaYF$_4$/TiO$_2$, (1 : 1)@(Yb,Er)-NaYF$_4$/C-TiO$_2$, and (Yb,Er)-NaYF$_4$ under the excitation of 980 nm laser and (d) overlap between the DRS and PL spectrum of (1 : 1)@(Yb,Er)-NaYF$_4$/C-TiO$_2$. For comparison, the DRS of (1 : 1)@(Yb,Er)-NaYF$_4$/TiO$_2$ was also indicated in (d).

visible light absorption of the samples improved with an increase in (Yb,Er)-NaYF$_4$ content. When the four kinds of samples in Figure 3(a) were excited by a NIR diode laser light (980 nm), different intensities of green light were emitted as shown in Figure 3(b). The (Yb,Er)-NaYF$_4$ powders showed the highest emission intensity with four emission peaks at about 408, 525, 540 and 653 nm, which are corresponding to the transitions from $^2H_{9/2}$, $^2H_{11/2}$, $^4S_{3/2}$ and $^4F_{9/2}$ to $^4I_{15/2}$ of Er^{3+}, respectively[37,38]. When the (Yb,Er)-NaYF$_4$ powders were mixed with undoped TiO$_2$ particles to form (1:1)@(Yb,Er)-NaYF$_4$/TiO$_2$, the relative emission intensity of peak at 540 nm decreased to about 1/4, probably due to the shielding of the excitation light by TiO$_2$ nanoparticles on the surface of (Yb,Er)-NaYF$_4$ core. More importantly, the relative emission intensity of sample (1:1)@(Yb,Er)-NaYF$_4$/C-TiO$_2$ declined more significantly. The reason for this dramatic decrement of emission intensity might be explained by Figure 3 (d). It could be explicitly observed that the DRS of (1:1)@(Yb,Er)-NaYF$_4$/C-TiO$_2$ had a good overlap with four emission peaks in PL spectrum, while no overlap could be observed for (1:1)@(Yb,Er)-NaYF$_4$/TiO$_2$, indicating that C-TiO$_2$ could efficiently absorb the visible fluorescence emitted from (Yb,Er)-NaYF$_4$. When the (1:1)@(Yb,Er)-NaYF$_4$/C-TiO$_2$ composite was excited by 980 nm laser, the up-conversion phosphor (Yb,Er)-NaYF$_4$ in the composite would emit green light with four emission peaks at 408, 525, 540 and 653 nm. Meanwhile, a large part of emitted green light would be efficiently absorbed by the C-TiO$_2$ particles coated on the surface of (Yb,Er)-NaYF$_4$, eventually leading to the strong reduction of emission intensity of green light compared with (Yb,Er)-NaYF$_4$ and (1:1)@(Yb,Er)-NaYF$_4$/TiO$_2$. As for sample C-TiO$_2$, no green light was observed when excited by 980 nm laser, since no up-conversion occurred in this sample. The corresponding visual emitting maps for these four samples monitored by 980 nm NIR light irradiation are presented in Figure 3 (c), in which the laser sources and IR light path are shown by computer graphics.

In order to investigate the status of C in the TiO$_2$ lattice, the XPS measurement was employed. From XPS spectra of C 1s for C-TiO$_2$ and (1:1)@(Yb,Er)-NaYF$_4$/C-TiO$_2$ in Figure 4, it could be obviously seen that both samples exhibited three peaks at 282.0 eV, 284.6 eV and 285.6 eV. The peak at 284.6 eV was ascribed to the adventitious carbon species from the XPS measurement and the peak around
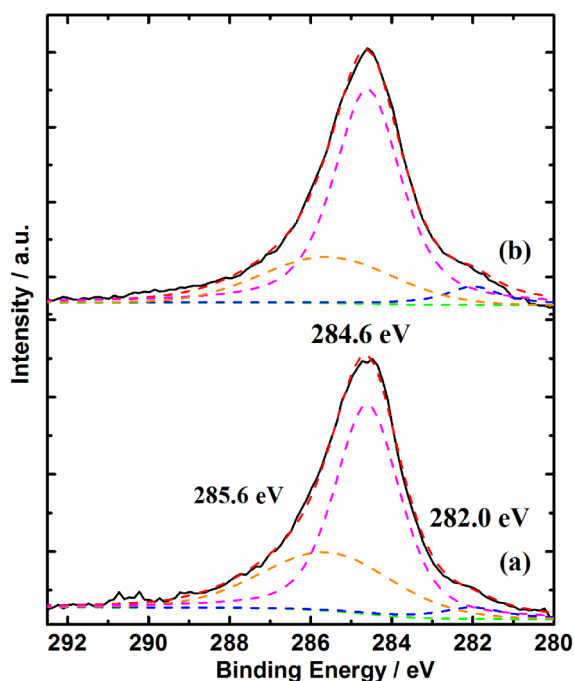
285.6 eV is corresponding to the elemental carbon which has the same binding energy as that of carbon in the graphite intercalation compound[39,40]. More importantly, the small peak at about 282.0 eV should be ascribed to the binding energy of C-Ti bond, indicating that the C had been successfully doped into TiO$_2$ lattice by replacing O site[31,41]. The relative area of 282.0 eV peak for (1:1)@(Yb,Er)-NaYF$_4$/C-TiO$_2$ was larger than that of C-TiO$_2$, and the corresponding doped C concentration for two samples were about 0.38 at.% and 0.19 at.%, which were well agreements with that of DRS result in Figure 3 (a). It is well known that some impurity C energy levels will be introduced above the valence band of TiO$_2$ when C was doped in O site of TiO$_2$, and then the electrons can be excited from impurity C energy levels instead of the valence band of TiO$_2$ to the conduction band of TiO$_2$, which eventually leads to the strong visible light absorption of C-TiO$_2$[16,17,30].

Photocatalytic activities. The photocatalytic activities of samples were investigated by testing the NO$_x$ gas destruction ability under the irradiation of UV, visible and NIR lights. Figure 5 illustrates the deNO$_x$ activity of various samples using different wavelengths of light sources and all of the samples were kept in dark for 30 min before irradiation to eliminate the influence of absorption of NO species by samples. In Figure 5 (A) and (C), it can be obviously seen that there was no obvious deNO$_x$ activity for (Yb,Er)-NaYF$_4$ (sample (c)) regardless of irradiation wavelengths. As for pure C-TiO$_2$ (sample (a)), 0%, 6.2%, 23.2%, 28.3% and 32.9% of NO were decomposed under the excitation of NIR diode laser, red LED, green LED, blue LED and UV LED, respectively. The nice visible light induced photocatalytic activity for this sample was mainly assigned to the excellent visible absorption of TiO$_2$ after C doping, but no NIR light driven deNO$_x$ activity was performed, because C-TiO$_2$ could not be excited by 980 nm NIR light. However, when C-TiO$_2$ photocatalyst was combined with (Yb,Er)-NaYF$_4$ up-conversion phosphor, about 8.5% of NO$_x$ gas was successfully destructed even when the NIR diode laser was used as the irradiation light source. This NIR light induced activity should be owing to the synergetic effect of C-TiO$_2$ photocatalyst and (Yb,Er)-NaYF$_4$ up-conversion phosphor, since no corresponding performance was observed by pure C-TiO$_2$ and (Yb,Er)-NaYF$_4$ individually. In addition, the visible light induced deNO$_x$ performance was significantly enhanced to 19.5%, 26.2% and 30% with the irradiation of 627, 530 and 445 nm LED lights, respectively. This interesting result might be dominantly due to the increased visible light absorption ability by increasing C doping content as shown in Figure 3(a). As for the effect of thermal reaction on the visible-NIR light induced photocatalytic activity, it could be ignored since no visible-NIR light responsive deNO$_x$ activity was observed for the pure (Yb,Er)-NaYF$_4$ and no NIR light driven deNO$_x$ performance was exhibited for solely C-TiO$_2$. Furthermore, the temperature was fixed at a constant room temperature during the photocatalytic testing.

The detailed mechanism for this synergy phenomenon will be explained in the following section. Besides, the deNO$_x$ activity of (1:1)@(Yb,Er)-NaYF$_4$/C-TiO$_2$ was also compared with those of (1:1)@(Yb,Er)-NaYF$_4$/TiO$_2$, (1:1)@(Yb,Er)-NaYF$_4$/N-TiO$_2$ and P25 using different wavelengths of lights (Figure 5(B)). When (Yb,Er)-NaYF$_4$ up-conversion phosphor was mixed with pure TiO$_2$, only 27.5% of UV light induced photocatalytic activity was displayed, and no distinct visible and NIR lights induced deNO$_x$ activity was presented due to the poor visible and NIR light absorption of pure TiO$_2$. As for P25, 26.8% and 9.6% of NO$_x$ were destructed when UV and blue LEDs were used as light sources, respectively. The XRD pattern, DRS and photoluminescence spectrum of (1:1)@(Yb,Er)-NaYF$_4$/N-TiO$_2$ are illustrated in supplementary Figure S4. The XRD profie of (1:1)@(Yb,Er)-NaYF$_4$/N-TiO$_2$ was similar to that of (1:1)@(Yb,Er)-NaYF$_4$/C-TiO$_2$, but the visible light absorption was much weaker, indicating only extend the

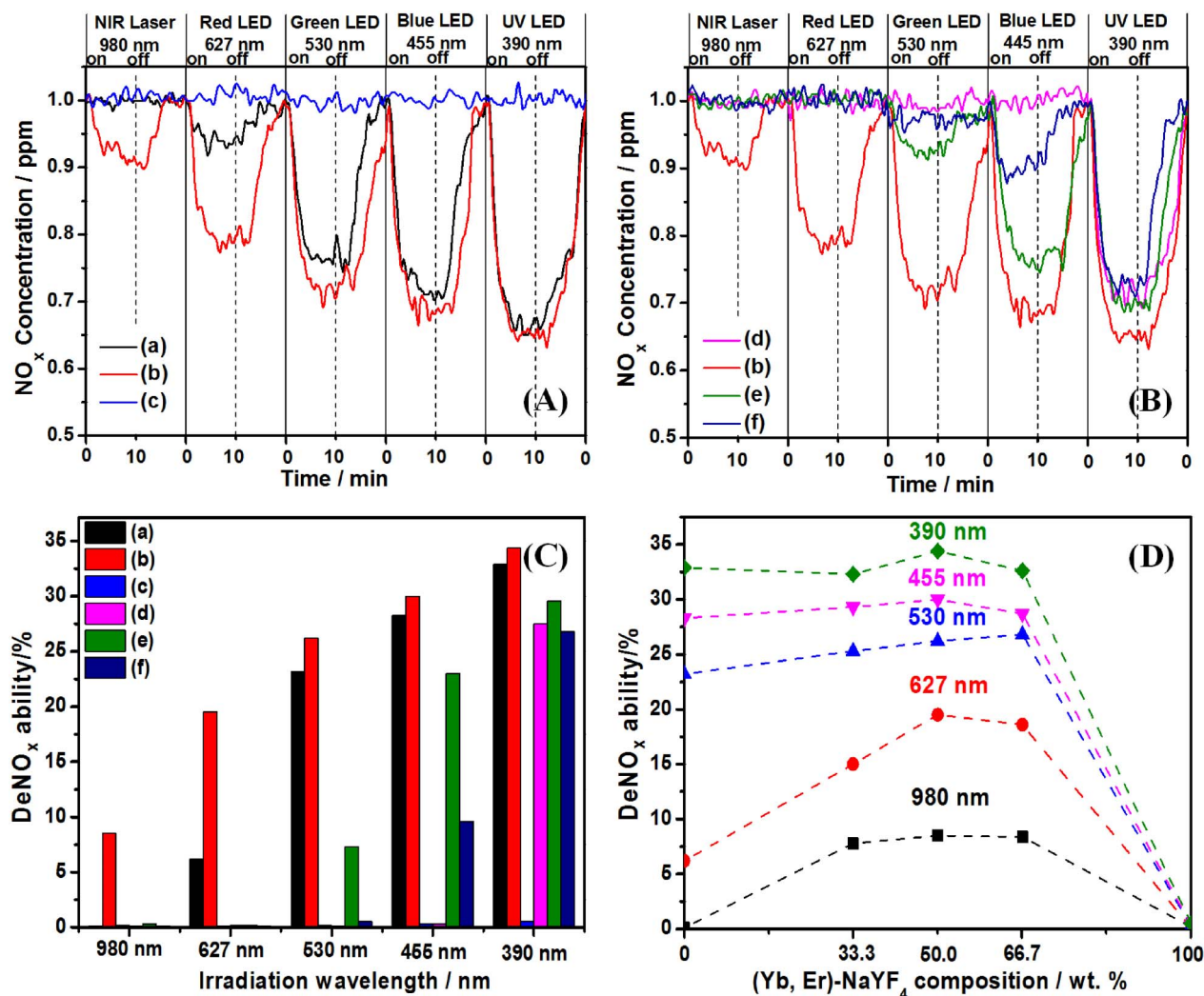**Figure 4 | XPS spectra of C1s for (a) C-TiO$_2$ and (b) (1:1)@(Yb,Er)-NaYF$_4$/C-TiO$_2$.**

Figure 5 | Time dependence of NO$_x$ destruction activity (A), (B), corresponding deNO$_x$ ability (C) of (a) C-TiO$_2$, (b) (1:1)@(Yb,Er)-NaYF$_4$/C-TiO$_2$, (c) (Yb,Er)-NaYF$_4$, (d) (1:1)@(Yb,Er)-NaYF$_4$/TiO$_2$, (e) (1:1)@(Yb,Er)-NaYF$_4$/N-TiO$_2$, (f) P25 titania under the irradiation of different wavelengths of lights, and the effect of (Yb,Er)-NaYF$_4$ content on the deNO$_x$ ability of (Yb,Er)-NaYF$_4$/C-TiO$_2$ composites (D).

absorption tail to about 560 nm. Consequently, (1:1)@(Yb,Er)-NaYF$_4$/N-TiO$_2$ exhibited only 7.3% and 23% of NO$_x$ destruction ability with the visible light irradiation of 530 and 445 nm, respectively. Although the absorption spectrum of (1:1)@(Yb,Er)-NaYF$_4$/N-TiO$_2$ showed a little overlap with its photoluminescence spectrum, it was still not effective enough to induce the obvious deNO$_x$ performance under the excitation of 980 nm light. Furthermore, the effect of (Yb,Er)-NaYF$_4$ content on the photocatalytic activity of (Yb,Er)-NaYF$_4$/C-TiO$_2$ composites was also studied using different wavelengths lights (in Figure 5-(D)). (1:1)@(Yb,Er)-NaYF$_4$/C-TiO$_2$ demonstrated a little better deNO$_x$ ability than those of other compositions of (Yb,Er)-NaYF$_4$/C-TiO$_2$ composites.

In addition, the deNO$_x$ ability of (1:1)@(Yb,Er)-NaYF$_4$/C-TiO$_2$ was also investigated by employing NIR laser, red LED, the combination of NIR laser and red LED as irradiation sources (Figure 6). It was clearly exhibited that about 19% of NO$_x$ gas was destructed under the excitation of red LED. While when NIR laser was combined with red LED as the light source, further 4.5% of NO$_x$ gas reduction was appeared and then moved back to 19% again as the NIR diode laser was eliminated. This result indicated that the NIR light induced deNO$_x$ ability of the C-TiO$_2$ photocatalyst combined with (Yb,Er)-NaYF$_4$ up-conversion phosphor truly had a positive effect on the total photocatalytic activity of photocatalyst when irradiated by UV, visible, NIR lights, therefore, the solar light might be more
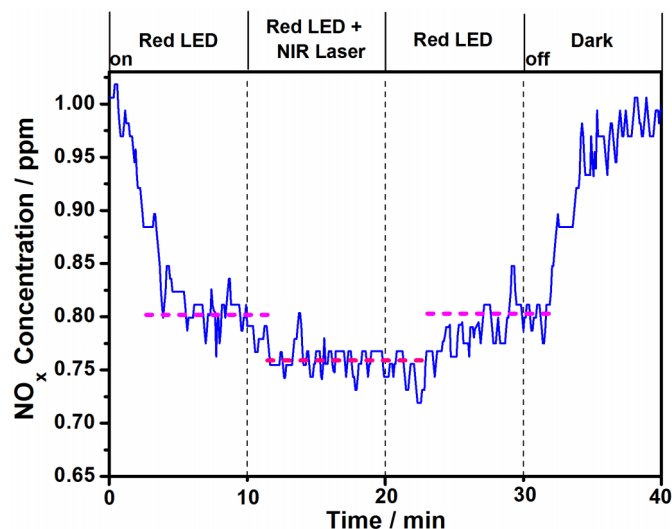

Figure 6 | DeNO$_x$ ability of sample (1:1)@(Yb,Er)-NaYF$_4$/C-TiO$_2$ with respect to the irradiation lights.

effectively utilized for photocatalysis compared with that of pure C-TiO$_2$ photocatalyst in the absence of up-conversion phosphor. Meanwhile, the dependence of deNO$_x$ ability of (1:1)@(Yb,Er)-NaYF$_4$/C-TiO$_2$ on the irradiation wattages of NIR diode laser is illustrated (see supplementary Figure S5). With an increase in irradiation wattage of NIR laser, the corresponding deNO$_x$ ability was increased, which further confirmed that the NIR light induced photocatalytic activity was actually realized and could be affected by irradiation energy power.

It is well known that the photoluminescence of phosphor is sensitive to the operating condition, and the surround atmosphere of the photocatalyst may change after irradiation for some time[42–44]. Therefore, the reproducibility of NIR light induced deNO$_x$ ability of (Yb,Er)-NaYF$_4$/C-TiO$_2$ composite was evaluated. The deNO$_x$ reaction performance of (1:1)@(Yb,Er)-NaYF$_4$/C-TiO$_2$ with the repeated induction of 980 nm light is shown in Figure 7. It is apparent that the NIR light induced deNO$_x$ ability of the sample presented no obvious difference after 4 times running, implying that the (Yb,Er)-NaYF$_4$/C-TiO$_2$ composite had an excellent stability for NO$_x$ destruction when irradiated by NIR light.

Discussion

Figure 8 illustrates the photoluminescence and UV, visible, NIR lights induced photocatalytic reaction mechanism of the (Yb,Er)-NaYF$_4$/C-TiO$_2$ composite. It is accepted that up-conversion phosphors can convert longer wavelength radiation (NIR light) to shorter wavelength fluorescence (UV or visible light) via a two-photon or multiphoton mechanism and then achieve the anti-stokes shift[45,46]. When a 980 nm NIR laser was used to excite the (Yb,Er)-NaYF$_4$/C-TiO$_2$, the Yb^{3+} as a sensitizer ion in (Yb,Er)-NaYF$_4$ phosphor could absorb this light, and then an electron was able to be excited from the $^2F_{7/2}$ to $^2F_{5/2}$ level. After that, the excited electron would transfer back to the ground state of $^2F_{7/2}$ and the released energy in this process was dominantly nonradiatively transferred to active ions of Er^{3+}, leading to a population of Er^{3+} from $^4I_{15/2}$ to $^4I_{11/2}$. In addition, a second or more similar 980 nm photons from excited Yb^{3+} ion could populate to much higher $^4F_{9/2}$, $^4F_{7/2}$ and $^2H_{9/2}$ energetic levels of Er^{3+} ion. Some of the excited electrons of Er^{3+} ion then would relax nonradiatively by a fast multiphonon decay process to the $^2H_{11/2}$, $^4S_{3/2}$, $^4F_{9/2}$ etc. energy levels. Finally, these excited electrons would radiatively transfer to the Er^{3+} ground state of $^4I_{15/2}$ and present four emissions at 408 nm
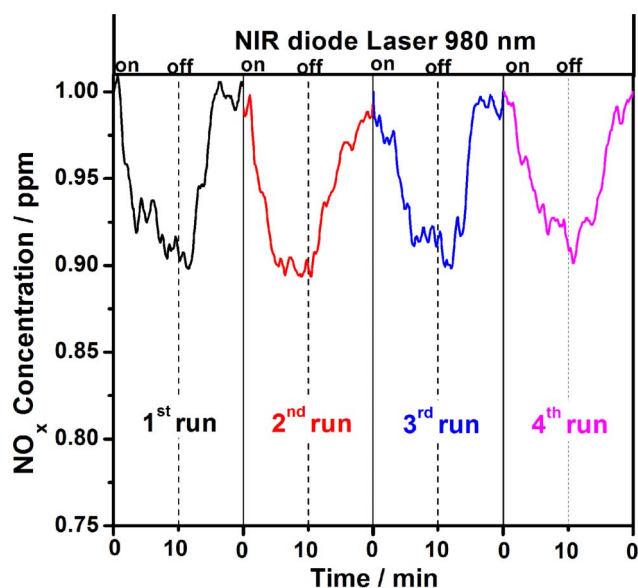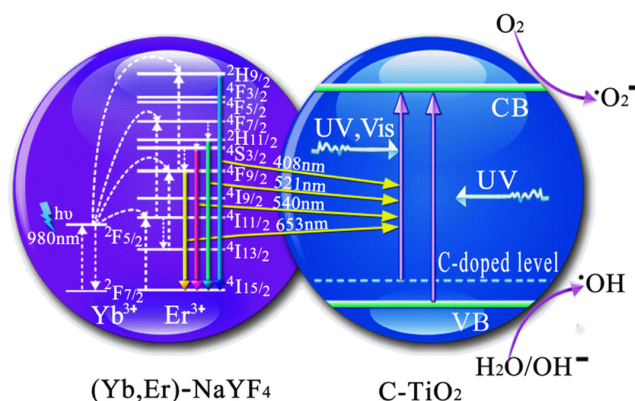

Figure 8 | Schematic illustration of the photoluminescence and photocatalytic mechanism of (Yb,Er)-NaYF$_4$/C-TiO$_2$ composite.

($^2H_{9/2} \rightarrow ^4I_{15/2}$), 521 nm ($^2H_{11/2} \rightarrow ^4I_{15/2}$), 540 nm ($^4S_{3/2} \rightarrow ^4I_{15/2}$) and 653 nm ($^4F_{9/2} \rightarrow ^4I_{15/2}$)[45,47]. The (Yb,Er)-NaYF$_4$ eventally emitted green light due to the main peak at 540 nm. In this case, the as-emitted green light from (Yb,Er)-NaYF$_4$ could be reabsorbed by the surface C-TiO$_2$ nanoparticles which had an excellent light absorption in the range of above mentioned four peaks owing to the C doping in TiO$_2$ (shown in Figure 3). At that time, the electron in TiO$_2$ was excited to the conduction band of TiO$_2$ from C doped impurity energy levels, producing a pair of hole and electron in TiO$_2$ lattice. The photogenerated hole would then be trapped by water and adsorbed OH$^-$ species in the air to generate hydroxyl radicals ·OH. Besides, the photoinduced electron in the conduction band would form ·O$_2^-$ in the presence of oxygen. In addition, the detailed destruction mechanism of NO species by photocatalyst has been investigated by some researchers[48–52]. The characterization system in the present research was quite similar to that of the Japanese Industrial Standard which was established at the beginning of 2004[54]. In this JIS standard, it is recommended that the photocatalytic activity of the photocatalyst should be characterized by measuring the decrease in the concentration of NO at the outlet of a continuous reactor. In the presence of oxygen, the electrons in the conduction band are immediately trapped by the molecular oxygen to form ·O^{2-}, which can then generate active ·OOH radicals[20,51,52]. The nitrogen monoxide reacts with these reactive oxygen radicals, molecular oxygen, and very small amount of water in the air to produce HNO$_2$ or HNO$_3$. It was reported that about 20% of nitrogen monoxide was decomposed to nitrogen and oxygen directly[53]. As for UV, visible lights induced photocatalytic performance of (Yb,Er)-NaYF$_4$/C-TiO$_2$ composite, it was very similar to that of NIR light induced activity. The only difference was that the irradiation light source for photocatalysis was not transferred from up-conversion phosphor but directly from the UV or visible light sources and then the electron would be excited from the valence band of TiO$_2$ or C doped energy levels to the conduction band of TiO$_2$, eventually inducing the photocatalysis.

In summary, the (Yb,Er)-NaYF$_4$/C-TiO$_2$ composites were successfully prepared by a simple calcination assisted solvothermal method. The results showed that when C-TiO$_2$ photocatalyst was combined with (Yb,Er)-NaYF$_4$ up-conversion phosphor, the visible absorption of C-TiO$_2$ was significantly improved up to 900 nm, which had a nicely overlap with the photoluminescence spectrum of (Yb,Er)-NaYF$_4$ excited by 980 nm. Due to this reason, the (Yb,Er)-NaYF$_4$/C-TiO$_2$ composite presented excellent deNO$_x$ ability not only under the irradiation of visible and UV lights but also NIR light, being much superior to those of pure C-TiO$_2$, P25 and even (Yb,Er)-NaYF$_4$/N-TiO$_2$ composite. In addition, the composite exhibited outstanding stability for the photocatalytic activity and truly played a positive effect in the improvement of utilization of total solar light

Figure 7 | The multi-cycles of deNO$_x$ ability of (1:1)@(Yb,Er)-NaYF$_4$/C-TiO$_2$ under the irradiation of 980 nm light.

(UV, visible, NIR lights) for photocatalysis. A promising strategy to utilize UV, weak visible lights and infrared light for photocatalysis simultaneously and effectively has been established. Furthermore, it also provides a strong potential to couple various color light-emitting up-conversion phosphors (such as blue, green, yellow, red emitting phosphors) with excellent visible light responsive C doped TiO_2 to form novel composites with high photocatalytic activity under the irradiation of UV, visible and infrared lights.

Methods

Sample preparation. A series of (Yb,Er)-$NaYF_4$/C-TiO_2 composites, with the (Yb,Er)-$NaYF_4$/C-TiO_2 weight ratios of 1 : 2, 1 : 1 and 2 : 1 were prepared by a simple calcination assisted solvothermal method, and were denoted as $(1:2)@(Yb,Er)$-$NaYF_4$/C-TiO_2, $(1:1)@(Yb,Er)$-$NaYF_4$/C-TiO_2, and $(2:1)@(Yb,Er)$-$NaYF_4$/C-TiO_2, respectively. The (Yb,Er)-$NaYF_4$ used in this experiment was purchased from Shanghai Huaming Gona Rare Earth New Materials Co., Ltd. (China). In a typical synthesis process of $(1:1)@(Yb,Er)$-$NaYF_4$/C-TiO_2 particle, The appropriate amounts of (Yb,Er)-$NaYF_4$ particles were dispersed in 20 mL ethanol with continuous stirring for 30 min. After that, 0.6 mL titanium tetra-n-butoxide was introduced dropwise to the suspension solution with another 30 min magnetic stirring. Subsequently, 10.5 mL ethanol/water (10 : 0.5) mixed solution was added dropwise to the solution and stirred for 60 min before transferring into a 100 mL Teflon-lined stainless steel autoclave. Finally, the solution was heated at $190°C$ for 2 h, and the products were separated by centrifugation, washed and calcined at $265°C$ for 1 h in ambient condition. For comparison, C-TiO_2 was prepared by a similar process without the addition of (Yb,Er)-$NaYF_4$ particles, and $(1:1)@(Yb,Er)$-$NaYF_4$/ TiO_2 without calcination at $265°C$.

For comparison, $(1:1)@(Yb,Er)$-$NaYF_4$/N-TiO_2 in which nitrogen doped titania $(N$-$TiO_2)$ was utilized instead of the carbon doped titania $(C$-$TiO_2)$ was also synthesized by a conventional hydrothermal method similar to our previous paper[20]. A desired amount of (Yb,Er)-$NaYF_4$, HMT (3 g, 99%) and 2 mL of 20 wt% $TiCl_3$ solution were mixed with 30 mL of distilled water. The mixture was placed into a stainless steel autoclave attached to a Teflon tube of internal volume of 100 mL. The autoclave was heated and kept at $90°C$ for 1 h to realize homogeneous precipitation and then heated at $190°C$ for 2 h. The powder product was separated by centrifugation, washed with distilled water and acetone three times, then vacuum dried at $80°C$ overnight. In order to eliminate the effect of organics remained in the sample, the dried particles were finally calcined at $450°C$ for 2 h.

Characterization. The crystalline phases of the products were identified by X-ray diffraction analysis (XRD, Bruker AXS D2 Phaser) using graphite-monochromized $CuK\alpha$ radiation. The UV–vis diffuse reflectance spectra (DRS) were measured using a UV–vis spectrophotometer (Shimadazu, UV-2450). The specific surface areas were determined by the BET method (Quantachrome Instruments, NOVA4200e). The size, shape and element mapping of the composites were observed by transmission electron microscopy (TEM, JEOLJEM-2010) and high resolution transmission electron microscopy (HRTEM) (FE-TEM, JEM-2100F). The chemical compositions of the samples were determined by the EDX spectrometer (Rayny EDX-800HS, Shimadzu). The surface composition and binding energy of the samples were determined by X-ray photoelectron spectroscopy (XPS, Perkin Elmer PHI 5600). The shift of the binding energy owing to relative surface charging was corrected using the C 1 s level at 284.6 eV as an internal standard and Ar^+ sputtering was employed to clean the surface of samples. Photoluminescence (PL) spectra of specimens were measured by a spectrofluorometer (Shimadzu RF-5300P).

Photocatalytic activity tests. The photocatalytic activities of samples were investigated by evaluating the decomposition of NO_x ($DeNO_x$) in a flow type reactor under irradiation of different wavelengths of LEDs and NIR laser (see supplementary Figure S6) at room temperature, where the detailed testing parameters were summarized in supplementary Table S1. The sample powder was spread in the hollow (20 mm $\times$ 16 mm $\times$ 0.5 mm) of a glass plate and then placed at the bottom center of the reactor (373 cm^3 of internal volume) in which a 1 : 1 mixed gas of air and nitrogen balanced 1 ppm of NO was flowed at the rate of 200 cm^3 min^{-1}. The sample powder was kept in the dark for 30 min to reach the adsorption and desorption equilibrium of NO gas. After that, the light source was turned on to irradiate the sample for 10 min and then turned off to recover to the original concentration for another 10 min. The measuring time for each sample under each light source was 20 min^{17}. The concentration of NO was monitored by a NO_x analyzer (Yanaco, ECL-88A) continuously. In addition, the testing temperature was kept at a constant room temperature by using an electric fan in an air conditioner room.

1. Kang, I. C. *et al.* Improvement in Photocatalytic Activity of TiO_2 under Visible Irradiation through Addition of N-TiO_2. *Environ. Sci. Technol.* **42**, 3622–3626 (2008).
2. Khan, S., Al-Shahry, M. & InglerJr, W. B. Efficient Photochemical Water Splitting by a Chemically Modified n-TiO_2. *Science* **297**, 2243–2245 (2002).
3. Yin, S., Zhang, Q., Saito, F. & Sato, T. Preparation of Visible Light-Activated Titania Photocatalyst by Mechanochemical Method. *Chem. Lett.* **32**, 358–359 (2003).
4. Rane, K. S. *et al.* Visible light-sensitive yellow $TiO_{2-x}N_x$ and Fe-N co-doped $Ti_{1-y}Fe_yO_{2-x}N_x$ anatase photocatalysts. *J. Solid State Chem.* **179**, 3033–3044 (2006).
5. Dong, Q. *et al.* Preparation of a new pyrochlore-type compound $Na_{0.32}Bi_{1.68}Ti_2O_{6.46}(OH)_{0.44}$ by hydrothermal reaction. *J. Solid State Chem.* **184**, 1899–1902 (2011).
6. Yin, S., Hasegawa, H., Maeda, D., Ishitsuka, M. & Sato, T. Synthesis of visible-light-active nanosize rutile titania photocatalyst by low temperature dissolution-reprecipitation process. *J. Photoch. Photobio. A* **163**, 1–8 (2004).
7. Chen, X. B., Liu, L., Yu, P. Y. & Mao, S. S. Increasing Solar Absorption for Photocatalysis with Black Hydrogenated Titanium Dioxide Nanocrystals. *Science* **331**, 746–750 (2011).
8. Yin, S., Wu, J. H., Aki, M. & Sato, T. Photocatalytic hydrogen evolution with fibrous titania prepared by the solvothermal reactions of protonic layered tetratitanate $(H_2Ti_4O_9)$. *Int. J. Inorg. Mater.* **2**, 325–331 (2000).
9. Tang, Y. N., Di, W. H., Zhai, X. S., Yang, R. Y. & Qin, W. P. NIR-Responsive Photocatalytic Activity and Mechanism of $NaYF_4$: $Yb,Tm@TiO_2$ Core-Shell Nanoparticles. *ACS Catal.* **3**, 405–412 (2013).
10. Qin, W. P., Zhang, D. S., Zhao, D., Wang, L. L. & Zheng, K. Z. Near-infrared photocatalysis based on YF_3 : Yb^{3+}, Tm^{3+}/TiO_2 core/shell nanoparticles. *Chem. Commun.* **46**, 2304–2306 (2010).
11. Wu, J. H. *et al.* A Novel Thermosetting Gel Electrolyte for Stable Quasi-Solid-State Dye-Sensitized Solar Cells. *Adv. Mater.* **19**, 4006-4011 (2007).
12. Duonghong, D., Borgarello, E. & Gratzel, M. Dynamics of light-induced water cleavage in colloidal systems. *J. Am. Chem. Soc.* **103**, 4685–4690 (1981).
13. Hwang, S. H., Kim, C. H. & Jang, J. S. SnO_2 nanoparticle embedded TiO_2 nanofibers - Highly efficient photocatalyst for the degradation of rhodamine B. *Catal. Commun.* **12**, 1037–1041 (2011).
14. Liu, R. Y., Hu, P. G. & Chen, S. W. Photocatalytic activity of Ag_3PO_4 nanoparticle/ TiO_2 nanobelt heterostructures. *Appl. Surf. Sci.* **258**, 9805–9809 (2012).
15. Ohno, T., Tanigawa, F. & Fujihara, K. Photocatalytic oxidation of water by visible light using ruthenium-doped titanium dioxide powder. *J. Photochem. Photobiol. A* **127**, 107–110 (1999).
16. Asahi, R., Morikawa, T., Ohwaki, T., Aoki, K. & Taga, Y. Visible-Light Photocatalysis in Nitrogen-Doped Titanium Oxides. *Science* **293**, 269–271 (2001).
17. Yin, S., Komatsu, M., Zhang, Q. W., Saito, F. & Sato, T. Synthesis of visible-light responsive nitrogen/carbon doped titania photocatalyst by mechanochemical doping. *J. Mater. Sci.* **42**, 2399–2404 (2007).
18. Sauvé, G. *et al.* Dye sensitization of nanocrystalline titanium dioxide with osmium and ruthenium polypyridyl complexes. *J. Phys. Chem. B* **104**, 6821–6836 (2000).
19. Zhou, W. J. *et al.* Ag_2O/TiO_2 Nanobelts Heterostructure with Enhanced Ultraviolet and Visible Photocatalytic Activity. *ACS Appl. Mater. Interfaces* **2**, 2385–2392 (2010).
20. Yin, S. *et al.* Synthesis of excellent visible-light responsive $TiO_{2-x}N_y$ photocatalyst by a homogeneous precipitation-solvothermal process. *J. Mater. Chem.* **15**, 674–682 (2005).
21. Li, C. H., Wang, F., Zhu, J. & Yu, J. C. $NaYF_4$: $Yb,Tm/CdS$ composite as a novel near-infrared-driven photocatalyst. *Appl. Catal. B: Environ.* **100**, 433–439 (2010).
22. Wei, Y., Lu, F. Q., Zhang, X. R. & Chen, D. P. Synthesis of Oil-Dispersible Hexagonal-Phase and Hexagonal-Shaped $NaYF_4$: Yb,Er Nanoplates. *Chem. Mater.* **18**, 5733–5737 (2006).
23. Heer, S., Kompe, K., Gudel, H. U. & Haase, M. Highly Efficient Multicolour Upconversion Emission in Transparent Colloids of Lanthanide-Doped $NaYF_4$ Nanocrystals. *Adv. Mater.* **16**, 2102–2105 (2004).
24. Sun, Y. J. *et al.* Controlled synthesis and morphology dependent upconversion luminescence of $NaYF_4$: Yb, Er nanocrystals. *Nanotechnology* **18**, 275609–275617 (2007).
25. Yu, X. F. *et al.* Dopant-Controlled Synthesis of Water-Soluble Hexagonal $NaYF_4$ Nanorods with Efficient Upconversion Fluorescence for Multicolor Bioimaging. *Nano. Res.* **3**, 51–60 (2010).
26. Zhang, F. *et al.* Uniform nanostructured arrays of sodium rare-earth fluorides for highly efficient multicolor upconversion luminescence. *Angew. Chem. Int. Ed.* **46**, 7976–7979 (2007).
27. Ren, W. *et al.* Low temperature preparation and visible light photocatalytic activity of mesoporous carbon-doped crystalline TiO_2. *Appl. Catal. B: Environ.* **69**, 138–144 (2007).
28. Huang, Y. *et al.* Effect of Carbon Doping on the Mesoporous Structure of Nanocrystalline Titanium Dioxide and Its Solar-Light-Driven Photocatalytic Degradation of NO_x. *Langmuir* **24**, 3510–3516 (2008).
29. Sakthivel, S. & Kisch, H. Daylight Photocatalysis by Carbon-Modified Titanium Dioxide. *Angew. Chem. Int. Ed.* **42**, 4908–4911 (2003).
30. Valentin, C. D., Pacchioni, G. & Selloni, A. Theory of Carbon Doping of Titanium Dioxide. *Chem. Mater.* **17**, 6656–6665 (2005).
31. Wang, X. *et al.* Multi-type carbon doping of TiO_2 photocatalyst. *Chem. Phys. Lett.* **444**, 292–296 (2007).
32. Wu, X. Y. *et al.* Synthesis of high visible light active carbon doped TiO_2 photocatalyst by a facile calcination assisted solvothermal method. *Appl. Catal. B: Environ.* **142–143**, 450–457 (2013).

33. Boulon, G. *et al.* Structural and Spectroscopic Characterization of Nominal Yb^{3+} : Ca$_8$La$_2$(PO$_4$)$_6$O$_2$ Oxyapatite Single Crystal Fibers Grown by the Micro-Pulling-Down Method. *Adv. Funct. Mater.* **11**, 263–270 (2001).

34. Martín-Rodríguez, R. *et al.* Upconversion Luminescence in Nanocrystals of Gd$_3$Ga$_5$O$_{12}$ and Y$_3$Al$_5$O$_{12}$ Doped with Tb^{3+}-Yb^{3+} and Eu^{3+}-Yb^{3+}. *J. Phys. Chem. C* **113**, 12195–12200 (2009).

35. Wang, D. H., Jia, L., Wu, X. L., Lu, L. Q. & Xu, A. W. One-step hydrothermal synthesis of N-doped TiO$_2$/C nanocomposites with high visible light photocatalytic activity. *Nanoscale* **4**, 576–584 (2012).

36. Wu, X. Y. *et al.* Photocatalytic Properties of Nd and C Codoped TiO$_2$ with the Whole Range of Visible Light Absorption. *J. Phys. Chem. C* **117**, 8345–8352 (2013).

37. Yi, G. S. *et al.* Synthesis, characterization, and biological application of size-controlled nanocrystalline NaYF$_4$: Yb, Er infrared-to-visible upconversion phosphors. *Nano. Lett.* **4**, 2191–2196 (2004).

38. Zeng, J. H., Su, J., Li, Z. H., Yan, R. X. & Li, Y. D. Synthesis and upconversion luminescence of hexagonal-phase NaYF$_4$: Yb, Er^{3+} phosphors of controlled size and morphology. *Adv. Mater.* **17**, 2119–2123 (2005).

39. Chen, C. *et al.* Preparation, characterization and visible-light activity of carbon modified TiO$_2$ with two kinds of carbonaceous species. *J. Mol. Catal. A: Chem.* **314**, 35–41 (2009).

40. Neumann, B., Bogdanoff, P., Tributsch, H., Sakthivel, S. & Kisch, H. Electrochemical Mass Spectroscopic and Surface Photovoltage Studies of Catalytic Water Photooxidation by Undoped and Carbon-Doped Titania. *J. Phys. Chem. B* **109**, 16579–16586 (2005).

41. Irie, H., Watanabe, Y. & Hashimoto, K. Carbon-doped Anatase TiO$_2$ Powders as a Visible-light Sensitive Photocatalyst. *Chem. Lett.* **32**, 772–773 (2003).

42. Kang, I. C., Zhang, Q. W., Yin, S., Sato, T. & Saito, F. Preparation of a visible sensitive carbon doped TiO$_2$ photo-catalyst by grinding TiO$_2$ with ethanol and heating treatment. *Appl. Catal. B: Environ.* **80**, 81–87 (2008).

43. Yan, S. C., Lv, S. B., Li, Z. S. & Zou, Z. G. Organic–inorganic composite photocatalyst of g-C$_3$N$_4$ and TaON with improved visible light photocatalytic activities. *Dalton Trans.* **39**, 1488–1491 (2010).

44. Chen, S. F., Yu, X. L. & Liu, W. Preparation and Photocatalytic Activity Evaluation of Composite Photocatalyst Fe-TiO$_2$/TiO$_2$. *ECS Trans.* **21**, 3–22 (2009).

45. Dai, Y. L. *et al.* Up-Conversion Cell Imaging and pH Induced Thermally Controlled Drug Release from NaYF$_4$: Yb^{3+}/Er^{3+}@Hydrogel Core-Shell Hybrid Microspheres. *ACS Nano.* **6**, 3327–3338 (2012).

46. Kang, X. *et al.* Core-Shell Structured Up-Conversion Luminescent and Mesoporous NaYF$_4$: Yb^{3+}/Er^{3+}@nSiO$_2$@mSiO$_2$ Nanospheres as Carriers for Drug Delivery. *J. Phys. Chem. C* **115**, 15801–15811 (2011).

47. Boyer, J. C. & van Veggel, F. Absolute Quantum Yield Measurements of Colloidal NaYF$_4$: Er^{3+},Yb^{3+} Upconverting Nanoparticles. *Nanoscale* **2**, 1417–1419 (2010).

48. Hoffmann, M. R., Martin, S. T., Choi, W. & Bahnemann, D. W. Environmental Applications of Semiconductor Photocatalysis. *Chem. Rev.* **95**, 69–96 (1995).

49. Sato, T., Zhang, P. & Yin, S. High Performance Visible Light Responsive Photocatalysts for Environmental Cleanup via Solution Processing. *Progress Cryst. Growth Character. Mater.* **58**, 92–105 (2012).

50. Yin, S., Slaeman, U. & Sato, T. Current Progress on Modified SrTiO$_3$ Visible Light Induced Photocatalyst. *Mater. Focus* **1**, 18–31 (2012).

51. Yin, S. *et al.* Photocatalytic Oxidation of NO$_x$ under Visible LED Light Irradiation over Nitrogen-Doped Titania Particles with Iron or Platinum Loading. *J. Phys. Chem. C* **112**, 12425–12431 (2008).

52. Dalton, J. S. *et al.* Photocatalytic oxidation of NO$_x$ gases using TiO$_2$: a surface spectroscopic approach. *Environ. Pollut.* **120**, 415–422 (2002).

53. Anpo, M. Development of the Second Generation Photocatalyst with Novel Functionality in the Ultraviolet and Visible Light. *Recent Developments on Visible Light Response Type Photocatalysts*, NTS Inc. (ed.), 3–42 (NTS, Tokyo, 2002).

54. Test Method for Air Purification Performance of Photocatalytic Materials - Part 1: Removal of Nitric Oxide, JIS R 1701-1:2004(J), (Japanese Standards Association, Tokyo, 2004).

Acknowledgments

Author contributions

X.W. and Q.D. conducted the most of investigation for the samples. X.W. wrote the main paper. S.Y. designed the concept and the experiment method of the research. S.Y. and T.S. supervised the project, had given valuable advices on the proceeding of this work, and revised the manuscript. B.L. and Y.W. had provided precious suggestions on the selection of up-converison phosphors. T.S. and S.L. led the GRL project and supported the characterization of the samples. All authors discussed the results and commented on the manuscript at all stages.

Additional information